Investigation of the Solvation Dynamics of an Organic Dye in Polar Solvents Using the Femtosecond Transient Grating Technique

Jean-Claude Gumy, Olivier Nicolet, and Eric Vauthey*

Institut de Chimie-Physique de l'Université de Fribourg, Pérolles, CH-1700 Fribourg, Switzerland

Received: July 1, 1999; In Final Form: October 11, 1999

The solvation dynamics of an organic dye, IR140, in methanol, ethanol, and in a series of six alkanenitriles has been investigated using the transient grating technique. In all solvents, the dynamics exhibit ultrafast, almost solvent-independent, components ascribed to inertial solvation, and a slower viscosity-dependent component, due to diffusive solvation. The relative amplitudes of these components depend on both the solvent and on the wavelength at which the experiment is performed. The contribution of inertial motion increases with decreasing size of the solvent molecules and with decreasing wavelength. It appears that diffusive motion is associated with a loose solvent shell, while inertial motion dominates when the solvation layer is dense.

Introduction

The role of the solvent is of primary importance for the chemical reactivity. First, the solvent can favor chemical reaction by transferring momentum to the reactive species. Second, solvent offers efficient channels to dissipate energy as heat. Indeed, many exoergic chemical reactions taking place in the condensed phase do not occur in the gas phase due to the lack of such energy dissipation channels. Third, the solvation energy is often a decisive factor for the occurrence of a given chemical process. In photochemistry, the nature of the lowest excited state can be switched by varying the polarity of the solvent.[1] Moreover, in the condensed phase, spectral features are broader in comparison to the gas phase. This is due to the fact that the measured spectrum corresponds to an ensemble averaging over many solute−solvent configurations.

The response of the nuclear contribution to the dielectric constant does not follow instantaneously a variation of the electric field, such as that accompanying a chemical reaction or an electronic transition. Until recently, it was thought that this solvation dynamics was a purely diffusive process.[2−4] This hypothesis was corroborated by measurement of the dynamics of the fluorescence Stokes shifts performed with picosecond laser pulses. The resulting solvation times were found to be of the same order of magnitude of the longitudinal dielectric relaxation times of the solvents. This parameter corresponds to the reorientational time of the solvent molecules under the influence of a constant charge and ranges from a few ps to several hundreds of ps, depending on the viscosity.[5] However, molecular dynamics simulations of dipolar solvation have revealed the importance of the inertial motion of the solvent molecules, which takes place on a time scale of a few tens to a few hundreds of femtoseconds and which can contribute to up to 80% of the solvent relaxation.[6] This prediction was verified afterward by Fleming and co-workers who performed time-resolved fluorescence Stokes shift measurements in acetonitrile with 125 fs pulses and later in water with 50 fs pulses.[7,8] Four and six wave-mixing techniques have also been shown to give insight into the solvation dynamics.[9−13] When the pulse duration is shorter than the electronic dephasing time of the probe molecule, photon echo techniques allow the disentanglement of homogeneous and inhomogeneous contributions to line broadening.[13,14] Fainberg and Huppert have shown that transient grating measurements with pulses longer than the dephasing time of the probe molecule can give information equivalent to those obtained from fluorescence Stokes shifts.[9] This can be understood in terms of transient hole-burning spectroscopy: by exciting the probe molecule with pulses which are shorter than the solvation time but longer than the dephasing time, i.e., which have a narrower spectrum than the absorption band of the probe molecule, only a subset of the ground state population is excited. This subset corresponds to probe molecules experiencing similar interactions with the solvent. Assuming that the ground-state recovery time of the probe molecule is much longer than the solvation processes, the spectral hole broadens as the thermal equilibrium distribution of solvent configurations is restored. Experimentally, this broadening can be monitored by measuring the decrease of the hole depth. While the fluorescence Stokes shift technique is limited to a few numbers of probe molecules, the transient grating technique approach can be carried out with any probe molecule. This is also valid for any other spectroscopy sensitive to absorbance changes, such as transient absorption or transient dichroism. Another important advantage of this method is that these measurements can be performed at various wavelengths, and thus various subsets of the ground-state population can be investigated. Low-temperature spectral hole-burning studies have shown that processes such as spontaneous hole refilling[15] or pressure-induced[16] and electric-field-induced[17] hole broadening are strongly dependent on the position of the hole in the inhomogeneous absorption band. Such investigations have revealed important information on the origin of line broadening in solids.

We report here on the study of the solvation dynamics of a dye, IR140, in methanol, ethanol and in a series of six alkanenitriles, from acetonitrile to decanenitrile, using the transient grating (TG) technique. While the solvation dynamics in alcohols and acetonitrile has been the subject of several investigations,[4,7,9,18−23] there is much less information on the solvation dynamics in longer alkanenitriles in a time scale less than 1 ps. Moreover, an investigation of the influence on the

* Corresponding author. E-mail: Eric.Vauthey@unifr.ch.

10.1021/jp992265+ CCC: $18.00
Published on Web 11/19/1999

solvation dynamics of the wavelength at which the experiment is performed is also reported.

Experimental Section

Apparatus. The pulses used for the TG measurements were generated by a cw mode-locked Ti:sapphire laser (Spectra-Physics, Tsunami) pumped by a Nd:YVO_4 laser (Spectra-Physics, Millenia V). The average output power at 800 nm was 900 mW at 82 MHz. The pulse duration measured at the sample position was between 65 and 75 fs fwhm. The output pulses were split into three parts, one probe and two pump pulses, with an intensity ratio of 1:10:10. The three pulses were sent along variable optical delay lines, before being focused onto the sample with a 90 mm achromatic lens. The three beams were arranged in a box configuration with a crossing angle of 5°. The delay lines for the pump pulses were only varied to optimize the temporal overlap and remained fixed during the measurements. The diffracted pulse was spatially isolated from the three other pulses with an iris located directly after the sample and recollimated with a 90 mm lens, before being sent to a photomultiplier tube (Hamamatsu R928). Its output was then directed to a computer board for digitization (Axiom AX5210 A/D board). The polarization of the pump and probe pulses was controlled with combinations of Glan-Taylor polarizers (Laser Components) and achromatic half-wave plates (Newport). A Glan-Taylor polarizer was also placed in front of the photomultiplier tube to select a precise polarization component of the signal.

To measure the dynamics at time delays longer than 50 ps, the picosecond TG setup described in ref 24 was used. In this case, the pump and probe wavelength was at 532 nm.

Samples. IR140 (Exciton) was used as received. Methanol (MeOH) and ethanol (EtOH) as well as acetonitrile (ACN) were of spectroscopic grade and used without further purification. Propionitrile (PrCN), butyronitrile (BuCN), valeronitrile (VaCN), octanenitrile (OcCN), and decanenitrile (DeCN) were washed twice with half the volume of concentrated HCl, then washed with saturated aqueous $NaHCO_3$, dried with $MgSO_4$, and distilled.[25] Unless specified, all products were from Fluka. For femtosecond TG, the concentration of IR140 was adjusted to obtain an absorbance at the pump wavelength of about 0.25 on 1 mm, the sample thickness. This corresponds to a concentration of about 1.5×10^{-5} M. The sample solutions were flowed at 3 mL/s in a home-built cell with 1.2 mm thick Suprasil windows (Helma 202-QS). The time required to replace the solution in the irradiated zone was of the order of 30 μs.

For the ps TG measurements at 532 nm, the concentration amounted to 2×10^{-4} M.

Results

Solvent Dependence. *Slow dynamics.* Figure 1A shows the TG signal measured at 532 with IR140 in PrCN. For these measurements, the crossed grating geometry was used, i.e., the pump pulses had perpendicular linear polarization, the polarization of the probe pulse was parallel to that of one pump pulse, and the signal polarizer was perpendicular to the probe polarizer.[24] This geometry prevents the formation of a density phase grating and a distortion of the time profiles at longer time delays.[26] The decrease of the diffracted intensity corresponds to the decay of the polarization grating via both rotational diffusion and ground-state recovery (GSR),[27]

$$I_{TG}^{CG} = I_0 \exp[-2k_{CG}t]k_{CG} = k_{rot} + k_{GSR} \qquad (1)$$

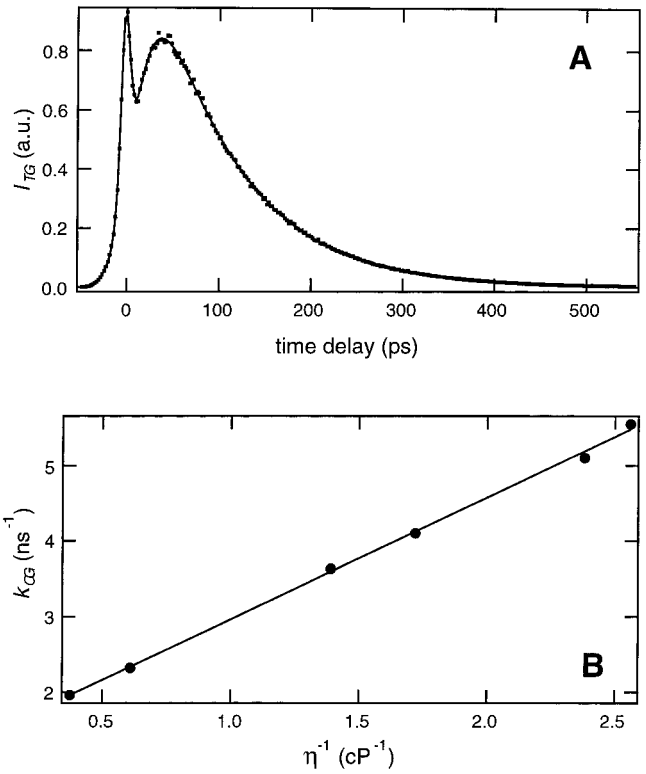

Figure 1. (A) Time profile of the diffracted intensity measured at 532 nm in PrCN using the crossed grating geometry (dots) and best fit of eqs 1 and 2 with an additional Gauss function (see text). (B) Viscosity dependence of the crossed grating decay rate constant, k_{CG}, in alkanenitriles.

where k_{rot} and k_{GSR} are the rate constants for rotational diffusion and GSR, respectively. The peak at time zero is the so-called coherence spike. It is due to the diffraction of one pump pulse off the grating formed between the probe pulse and the other pump pulse at time zero.[28,29] This spike occurs in any pump−probe experiments when the probe and pump pulses are at the same wavelength and derived from the same pulse.

The TG intensity, I_{TG}, can be expressed as[30,26]

$$I_{TG}(t) \propto \int_{-\infty}^{+\infty} I_{pr}(t - t')[\int_{-\infty}^{t} \chi^{(3)}(t'' - t')I_{pu}(t')\,dt']^2\,dt'' \qquad (2)$$

where I_{pr} and I_{pu} are the probe and pump intensities and $\chi^{(3)}$ is the third-order nonlinear susceptibility of the sample. $\chi^{(3)}$ is a third rank tensor whose elements correspond to various orientations of the four electric fields. The crossed grating geometry is therefore sensitive to $\chi^{(3)}_{1212}$. Various processes can contribute to $\chi^{(3)}$:[26] the electronic and the nuclear Kerr effects (OKE) from the solvent, the formation of population gratings, and the generation of a density phase grating due to heat releasing processes. In all the TG data presented here, there is no contribution from the OKE of the solvents. Moreover, the contribution of the density phase grating to $\chi^{(3)}_{1212}$ is zero, as such a grating is not formed in the crossed grating geometry, the pump intensity not being spatially modulated. Consequently, the signal intensity is only due to population gratings.

To fit properly eq 2 to the data shown in Figure 1A, $\chi^{(3)}_{1212}$ had the following functional form:

$$\chi^{(3)}_{1212}(t) = I \exp(-k_{CG}t) \qquad (3)$$

To account for the coherent spike, an additional Gaussian function centered at time zero was used. This Gaussian was

TABLE 1: Best Fit Parameters of Eqs 2 and 4 with an Additional Gaussian to the Measured TG Profiles Measured at 800 nm in Various Solvents[a]

solvent	A_G	$\Delta\tau_G$ (fs)	A_1	τ_1 (fs)	A_2	τ_2 (ps)	A_3	τ_3 (ps)
MeOH	0.180	65	0.166	256	0.197	5.7	0.444	240
EtOH	0.196	66	0.151	225	0.227	10.5	0.415	434
ACN	0.141	47	0.230	180	0.141	2.0	0.472	179
PrCN	0.135	45	0.227	190	0.140	2.7	0.483	196
BuCN	0.137	50	0.226	195	0.164	3.8	0.457	243
VaCN	0.151	49	0.191	203	0.180	4.7	0.462	285
OcCN	0.163	45	0.174	187	0.176	6.4	0.471	430
DeCN	0.194	56	0.144	196	0.172	8.9	0.474	510

[a] A_4,τ_4, and ω are essentially independent on the solvent and amount to 0.02, 500 fs, and 23 ps^{-1}, respectively. The τ_3 values have been determined from the fit of eqs 2 and 3 to the slow dynamic data ($\tau_3 = k_{CG}^{-1}$).

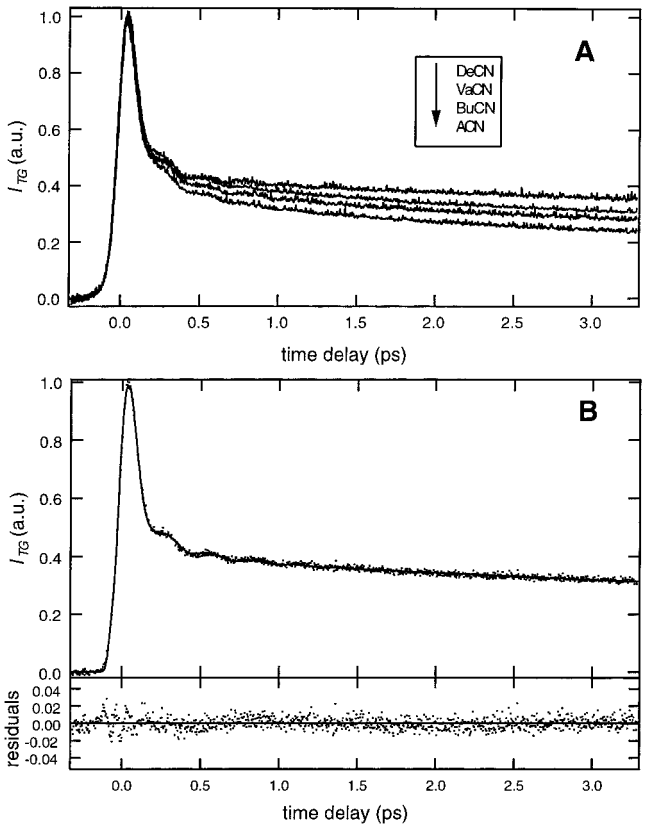

Figure 2. (A) TG decays at 800 nm measured in several alkanenitriles using the crossed grating geometry. (B) TG decay at 800 nm measured in EtOH using the crossed grating geometry, best fit of eqs 2 and 4 with an additional Gauss function and residuals.

simply added to the convolution of $\chi^{(3)}_{1212}(t)$ with the pump pulse profile. The result was then squared and convoluted with the probe pulse profile. It can be seen that this simple treatment of the coherent coupling spike results in a good fit. Moreover, the relative intensities of the coherent spike and incoherent signal at time zero have a ratio close to 4:1, as predicted by theory.[28,29] The k_{CG} values obtained from the fit are listed in Table 1. Figure 1B shows a plot of k_{CG} in alkanenitriles as a function of $1/\eta$, where η is the solvent viscosity. From the intercept of the linear fit, the rate constant of GSR, k_{GSR}, amounts to 1.35 ± 0.6 ns^{-1}.

Fast Dynamics. Figure 2 shows TG decays measured at 800 nm in nitriles and in EtOH with the femtosecond setup using the crossed grating geometry. The time profiles look biphasic, with an initial spike and a slower decay. The initial part of the decay does not exhibit a strong solvent dependence. Moreover, an oscillation with a solvent-independent frequency is observed.

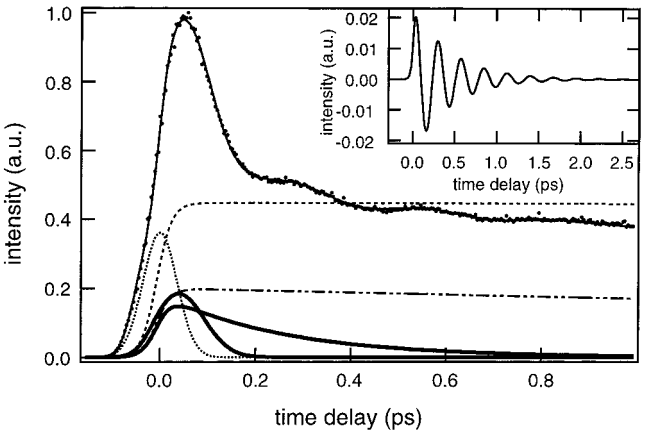

Figure 3. Relative contributions to the diffracted intensity measured at 800 nm in MeOH (dots): inertial solvent motion (Gaussian and exponential functions, bold), diffusive solvent motion (exponential function, dotted-dashed), population and rotational relaxation (exponential function, dashed), wave packet motion (damped cosine function, insert), and coherent coupling spike (Gaussian function, dotted). For the fit, the five contributions are added and squared and the result is convoluted with the probe pulse profile.

These decays are qualitatively very similar to those reported by Fleming and co-workers[22] as well as Huppert and co-workers[9] using the same technique. To fit properly eq 2 to these data, the following functional form has to be used for $\chi^{(3)}_{1212}(t)$:

$$\chi^{(3)}_{1212}(t) = A_G \exp[-(t/\Delta\tau_G)^2) + \sum_{i=1}^{3} A_i \exp(-t/\tau_i) + A_4 \exp(-t/\tau_4) \cos(\omega t + \phi) \quad (4)$$

where the first term is the Gaussian function reproducing the initial peak and the last term is a damped cosine function reproducing the oscillation of the TG intensity. At least three exponentials are required for a proper fit, the slowest one having a lifetime $\tau_3 = k_{CG}^{-1}$. For the fit, the pump and probe pulses were taken as Gaussian. The best fit was obtained by letting the pulse duration vary during the fit. However, the resulting duration was substantially larger than that measured by autocorrelation at the sample position. When the measured duration was kept fixed, the fit was very good in the decaying part of the signal but was poorer on the rising edge. We attribute this effect to the contribution of coherent coupling spike to the signal. This coherent coupling effect has been invoked by Cong et al. to explain the initial spike in GSR measurements such as those shown in Figure 2.[31] However, Fleming and co-workers have shown that this spike arises almost entirely from the ultrafast solvation dynamics.[22] An excellent fit to the data is obtained with the measured pulse duration, if an additional Gaussian function centered at time zero is used, as described above for the ps TG signals. The various contributions to the signal are shown in Figure 3. The parameters obtained from the fit are listed in Table 1 together with the fixed parameter τ_3. The oscillation amplitude, A_4, frequency, ω, and the damping time, τ_4, amount to about 0.02, 23 ps^{-1}, and 500 fs, respectively, in all solvents investigated.

Without going into detail, this table shows that the width of the Gaussian function, $\Delta\tau_G$, is in both solvent series less than 70 fs, i.e., close to the pulse duration ($\Delta\tau$(fwhm) $= 1.66\Delta\tau_G$). A fast exponential with a lifetime,τ_1, around 250 and 200 fs is observed in alcohols and in nitriles, respectively. Neither $\Delta\tau_G$ nor τ_1 shows any viscosity dependence. However, the lifetime, τ_2, associated with the second exponential exhibits a marked

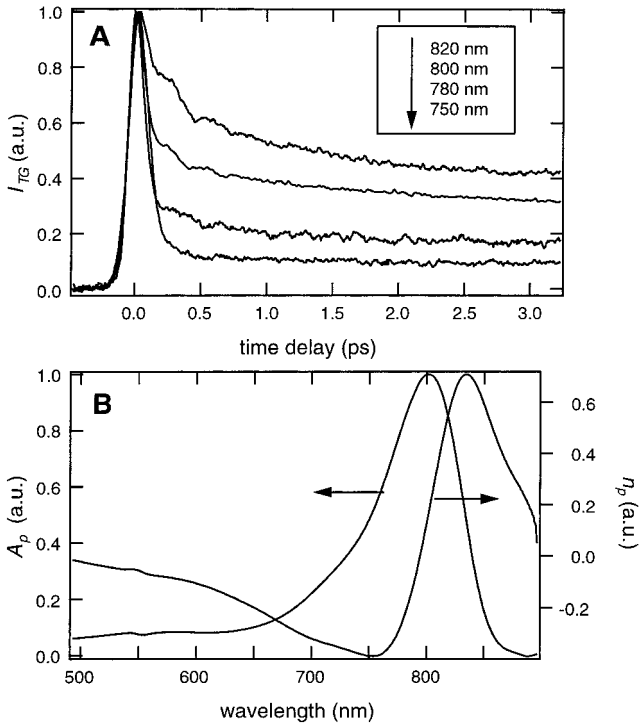

Figure 4. (A) TG decays measured at various wavelengths in MeOH with parallel polarization of the four beams. (B) Absorption and calculated dispersion spectra of IR140 in MeOH.

viscosity dependence and goes from 2 ps in ACN to about 10 ps in EtOH and in DeCN.

Wavelength Dependence. The variation of the TG decay with wavelength strongly depends on the polarization of the four interacting beams. TG decays recorded at various wavelengths with all parallel polarization of the beams are shown in Figure 4A. Two types of changes can be observed: (i) the intensity ratio of the initial spike to the slow decay increases by going from the red to the blue wavelength and (ii) the lifetimes associated with the various components vary substantially with the wavelength. A slow rise is even observed at 750 nm.

This spectacular effect is ascribed to the interference of the population phase grating with an accumulated density phase grating. This density phase grating is due to the thermal expansion following nonradiative deactivation of the excited state.[32] The lifetime of the grating depends on the fringe spacing, around 9 μm in the present case, and on the thermal diffusivity of the sample solutions, which is of the order of 10^{-7} m^2/s. This results in a density grating lifetime of about 20 μs. With parallel polarizations, the diffracted intensity is proportional to $|\chi^{(3)}_{1111}|^2$, where $\chi^{(3)}_{1111}$, which contains contributions from population gratings and density grating, is a complex quantity:

$$\text{real}(\chi^{(3)}_{1111}) = \chi^{(3)}_{1111}(\Delta n_p) + \chi^{(3)}_{1111}(\Delta n_d) \quad (5a)$$

$$\text{imag}(\chi^{(3)}_{1111}) = \chi^{(3)}_{1111}(\Delta A_p) \quad (5b)$$

where $\chi^{(3)}_{1111}(\Delta n_p)$ and $\chi^{(3)}_{1111}(\Delta n_d)$ are responsible for variation of refractive index due to population, Δn_p, and density changes, Δn_d, respectively, while $\chi^{(3)}_{1111}(\Delta A_p)$ is connected to the variation of absorbance due to population changes, ΔA_p. From eqs 2 and 5a, it is clear that the signal generated by both phase gratings can interfere. The intensity and the nature of the interference depend on the relative magnitude and sign of Δn_p and Δn_d and on the associated tensor elements, $\chi^{(3)}_{1111}$.[32−34] The

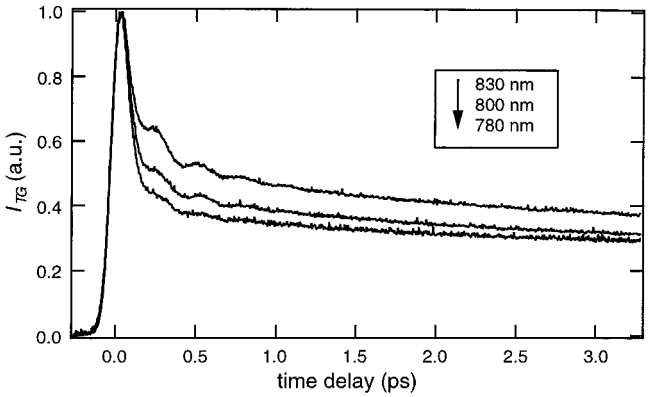

Figure 5. TG decays measured at various wavelengths in MeOH using the crossed grating geometry.

change of refractive index is caused by thermal expansion following heat release, and thus Δn_d is negative. On the other hand, Δn_p can be obtained by Kramers−Kronig transformation of ΔA_p. Figure 4B shows the absorption spectrum, $A_p(\lambda)$, and the calculated dispersion spectrum, $n_p(\lambda)$, of IR140 in MeOH. If we assume that, the photoinduced absorbance change in this spectral region is only due to the bleaching of IR140 ground state absorption, ΔA_p and Δn_p are simply proportional to $-A_p$ and $-n_d$, respectively. From this figure, it appears that Δn_p is negative on the red side of the absorption band and positive on the blue side. Thus, the interference between the density and the population phase gratings should be constructive at wavelengths longer than 800 nm and destructive at lower wavelengths. Moreover, there should be no interference at 800 nm, where Δn_p vanishes. This is in perfect agreement with the observation. Indeed, the light diffracted by the accumulated density phase grating acts as a local oscillator, in phase with the light diffracted by the population phase grating, but in quadrature with the light diffracted from the population amplitude grating. The resulting signal is a mixture of heterodyne and homodyne signals. The heterodyne signal scales linearly with Δn_p and contains information on its sign, while the homodyne signal scales quadratically with ΔA_p and is always positive. For these reasons, the signal at 800 nm ($\Delta n_p = 0$) is identical to the signal measured with the crossed grating configuration ($\Delta n_d = 0$). Similarly, this explains why the apparent decay of the signal at $\lambda > 800$ nm (constructive interference) is slower than at 800 nm and why the decay at $\lambda < 800$ nm is faster (destructive interference).

These results also confirm that the absorbance changes around 800 nm are due to the bleaching of the ground state absorption only. If the excited-state absorption were also involved, the resulting absorption change spectrum would be different from $-A_p$, displayed in Figure 4B, and Δn_p would not vanish at 800 nm. Consequently, the TG decay at this wavelength would not be the same in the crossed grating and in the all parallel polarization geometry.

Figure 5 shows the TG decays measured at several wavelengths between 830 and 780 nm in MeOH using the crossed grating geometry, i.e., without the formation of an accumulated density grating. For these measurements, great care was taken to keep the pulse duration, the pulse energy, and the sample absorbance constant. These decays were analyzed using eqs 2 and 4 with the additional Gauss function. In this case, the lifetimes τ_1 to τ_3, the width of the Gaussian $\Delta\tau_G$, as well as the parameters pertaining to the oscillation, A_4, τ_4, and ω, obtained from the fit were independent of the wavelength. The effect of wavelength appears only in the relative amplitudes A_G to A_3, as shown in Table 2.

TABLE 2: Best Fit Parameters of Eqs 2 and 4 with an Additional Gaussian to the Measured TG Time Profiles Measured in MeOH at Various Wavelengths[a]

λ (nm)	A_G	$\Delta\tau_G$ (fs)	A_1	τ_1 (fs)	A_2	τ_2 (ps)	A_3
830	0.107	58	0.169	260	0.239	6.3	0.471
820	0.115	60	0.158	259	0.256	6.3	0.465
800	0.184	66	0.148	254	0.197	6.4	0.450
780	0.240	64	0.138	231	0.150	6.5	0.454

[a] A_4,τ_4, ω are essentially independent on λ and amount to 0.02, 500 fs, and 23 ps^{-1}, respectively. τ_3 has been fixed to 240 ps.

This table shows that the amplitude of the Gaussian component increases with decreasing wavelength, while A_1 decreases only weakly. On the other hand, the amplitude of the slower, viscosity-dependent component, A_2, shows a strong decrease from the red to the blue, and the relative amplitude associated with the long decay time, τ_3, decreases weakly.

Discussion

The GSR signals contains four contributions.

(i) The contribution due to the decay of the polarization grating with a lifetime τ_3 determined with the picosecond TG experiment at 532 nm ($\tau_3 = k_{CG}^{-1}$).

(ii) The contribution due to solvation, i.e., the restoration of the equilibrium distribution of solvent configurations after depletion of a subset of these configurations. This contribution is phenomenologically described by a Gaussian and two exponential functions with decay time τ_1 and τ_2, respectively.

(iii) The contribution from the propagation of a ground state wave packet generated via impulsive stimulated Raman scattering. This contribution is described by a frequency, ω, and a damping time, τ_4, which are independent of both the solvent and the wavelength.

(iv) The contribution of the coherence coupling spike at zero time delay, which is present in all pump−probe experiments performed at a single wavelength.

The latter contribution is of course unwanted but cannot be avoided. As discussed in the previous section, we think that this spike has been accounted for by adding a Gaussian function centered at time zero. As this procedure gives good results with the picosecond TG data shown in Figure 1, it should work as well for the ultrafast TG data. Consequently, the contribution of the coherent coupling to A_G must be negligible. This is in agreement with the wavelength dependence of the GSR signal. According to Cong et al., the amplitude of the coherence coupling spike increases as the wavelength at which the experiment is performed is located further apart from the absorption band maximum.[31] This means that, if A_G was dominated by the coherent coupling, it should decrease from 830 nm to about 810 nm, and then increase again when going to a shorter wavelength. As shown in Table 2, this behavior is not observed, A_G increasing continuously from 830 to 780 nm. However, the amplitude of the added Gaussian function decreases weakly from 830 to 800 nm (from 0.44 to 0.41) and increases again at 780 nm to 0.42, in agreement with the prediction of Cong et al.[31] Nevertheless, this variation is close to the error limit and could be coincidental.

Solvent Dependence. As shown in Table 1, the total contribution of solvation to the signal, $A_s = A_G + A_1 + A_2$, is almost constant in a given solvent series. The contribution of solvation to the GSR signal can be separated into two parts: the contribution of inertial motion, which does not depend on viscosity, and the contribution of diffusive motion, which is viscosity dependent. The inertial contribution is accounted for by the initial Gaussian and the fastest exponential decay, while the diffusive solvation is described by the single exponential with a decay time τ_2. These τ_2 values in MeOH and EtOH are in good agreement with those reported in the literature.[4,21] In ACN, the τ_2 value is very similar to that of 2.23 ps reported recently by Passino et al.[23] The solvation times in PrCN, BuCN, and VaCN are also of the same order of magnitude as those previously published, i.e., between 2 and 4 ps.[4] To our knowledge, there are no data on the solvation dynamics in OcCN and DeCN.

There is also less data concerning the faster contributions to solvation. In the alcohols, the width of the Gaussian amounts to about 65 fs. The lifetime of the first exponential, τ_2, is also the same in both alcohols and lies around 240 fs. Lifetimes of the order of 400 fs have been reported by Goldberg et al.[9] Horng et al. have observed an exponential with a similar time constant in the solvation dynamics of a coumarin in a series of alcohols.[21] Moreover, recent three pulse stimulated photon echo peak shift (3PEPS) measurements performed on DTCI in MeOH showed a 260 fs component.[35] On the other hand, similar 3PEPS investigations of the solvation dynamics of IR144 did not reveal any component between 100 fs and 1 ps in both MeOH and EtOH.[23] The origin of these differences is not understood and could be related to the nature of the probe molecule.

Although τ_G and τ_1 do not exhibit an apparent solvent dependence in a given series, the situation is different if the amplitudes A_G, A_1, and A_2 are considered. In alcohols, A_G and A_1 are almost constant while A_2 increases by going from MeOH to EtOH.

In the nitriles, the width of the initial Gaussian is somewhat smaller than in the alcohols and is of the order of 50 fs. Similarly, τ_1 is smaller than in the alcohols and lies around 190 fs. A 90 fs and a 630 fs component have been reported for coumarin in ACN by Horng et al.,[21] while Passino at al. have found 73 fs and 2.23 ps components with IR144.[23] Finally, Lee et al. have reported 219 fs and 2.1 ps components with DTCI in ACN,[35] in good agreement with the present results. Concerning the amplitudes, A_G increases with increasing length of the solvent molecule, while A_1 exhibits the opposite behavior. A similar trend can be found in the data reported by Horng et al. The relative amplitude of the component around 300 fs decreases from 0.34 to 0.07 by going from MeOH to decanol.[21] The sum of the amplitudes related to inertial solvation, $A_G + A_1$ decreases with increasing length of the solvent molecules. This effect is confirmed by the increases of A_2 with increasing chain length. Molecular dynamics simulations of solvation indicate that the inertial contribution is largely due to the molecules located in the first solvation shell.[36] For small solvent molecules, inertial motion can involve the rotation of the whole molecule. For longer molecules, only the polar heads must contribute to the inertial motion. Consequently, it is reasonable to assume that inertial solvation is more efficient in solvents such as ACN or MeOH, where the number of polar heads around the solute molecule is large, than in long nitriles and alcohols, where substantial reorientation of the solvent molecules cannot occur without diffusional motion.

Wavelength Dependence. The wavelength dependence measured with parallel polarization is due to a large extent to interference between the signals originating from the population and density phase gratings. However, the wavelength dependence measured in the crossed grating configuration is not "contaminated" by this effect. This is confirmed by the fact that the dynamics parameters obtained from the fit, $\Delta\tau_G$ to τ_2,

did not show significant wavelength dependence. Table 2 shows that the total contribution of solvation to the signal, $A_s = A_G + A_1 + A_2$, increases weakly with decreasing wavelength. This is in agreement with theoretical prediction by Joo et al.[22] This effect can be explained by the dynamic Stokes shift in the GSR process. Indeed, the minima of the ground and excited potentials are not located at the same position. Thus, GSR occurs from the minimum of the excited state potential to the edge of the ground state potential, which corresponds to the red side of the absorption spectrum.

Larger wavelength effects can be observed in the relative amplitudes related to the solvation dynamics. Indeed, A_G exhibits a strong increase, by a factor larger than 2, with decreasing wavelength. As explained above, this confirms that the coherent coupling spike does not contribute significantly to A_G. On the other hand, A_1 shows only a very weak decrease, by a factor 1.2, by going from 830 to 780 nm. Finally, the amplitude of the diffusive solvation, A_2, shows a decrease by a factor 1.6.

There are only very few reports on the wavelength dependence of solvation dynamics. Such an investigation is not possible with fluorescence Stokes shift measurements. Moreover, the spectrum associated with pulses shorter than 25 fs, as used in some groups, is so large ($\Delta\lambda > 36$ nm around 800 nm) that it almost entirely overlaps with the absorption band of the probe molecule. Heterodyne transient dichroism measurements with rhodamine 800 (R800) in H_2O at two wavelengths have been reported by Zolotov et al.[37] The data (Figure 3 in ref 37) show that the initial spike increases with decreasing wavelength, while the amplitude of the slower component decreases. However, the pulse duration was not exactly the same for both measurements.

The wavelength dependence observed with IR140 indicates that the different positions within the absorption band of the probe molecule correspond to different solvent configurations with different dynamics. The solvent configurations for the red side involve more diffusional motion than the configurations corresponding to blue side absorption. Interestingly, the absorption band of IR140 is shifted to a shorter wavelength as the polarity of the solvent increases. For example, the absorption maximum goes from 811 nm in OcCN ($\epsilon = 13.9$) to 802 in ACN ($\epsilon = 37.5$). The same trend is observed in the alcohols. Coming back to the absorption band of IR140 in MeOH, these data imply that the molecule is better solvated when absorbing in the blue part of the band than when absorbing at longer wavelengths. Moreover, a compact and dense solvent shell will also result to shorter wavelength absorption than a looser and less dense shell. It is therefore quite reasonable to assume that inertial motion is much more important in the dense solvent shell than in the loose one. The latter configuration corresponds to instants where solvent molecules are diffusing and leave some free space around the solute. This could explain why solvation dynamics is dominated by diffusive motion at 830 nm and by inertial motion at 780 nm. A good proof of this model would be the observation of the opposite wavelength dependence with a probe molecule exhibiting a red shift of the absorption band with increasing solvent polarity. Such a probe molecule absorbing around 800 nm could not be found. All molecules with an absorption spectrum suitable to our laser also showed a blue shift with increasing solvent polarity. Moreover, TG measurements performed with two of them (1,1′diethyl-2,2'tricarbocyanine perchlorate and 1,1′diethyl-2,2′dicarbocyanine iodide) reveal qualitatively the same wavelength dependence as for IR140. However, the first absorption band of the dye R800, studied by Zolotov et al., shifts from 680 nm in acetone ($\epsilon = 20.7$) to 687 nm in dimethylformamide ($\epsilon = 36.7$).[37] As mentioned above, the wavelength dependence of the solvation dynamics of R800 seems to be the reverse of that observed with IR140, as would be expected by our hypothesis.

Conclusion

This investigation shows that the TG technique is well suited for investigating ultrafast solvation processes under the following conditions.

(i) Crossed grating geometry has to be used when working at high repetition rate to avoid interference effects with an accumulated thermal grating. Interference can also be avoided when working at a wavelength where the refractive index variation associated with the absorbance change is zero. This wavelength corresponds to the maximum of the absorption band of the probe molecule, as long as there is no transient absorption is this region.

(ii) The contribution of the coherent coupling must not be neglected. However, its relative contribution to the signal appeared to be basically independent of both the solvent and the wavelength.

(iii) In order to investigate the wavelength dependence of the solvation dynamics, the laser pulse duration should not be too short, to allow selective excitation within the broadened absorption band of the probe molecule.

The advantage of this technique over the fluorescence Stokes shift measurements is the possibility to perform measurements at different wavelengths within the absorption band of the probe molecule. The wavelength dependence of the solvation dynamics allows a new insight into the line broadening process to be gained. From the results obtained here, it appears that diffusional solvent motion is associated with a loose solvent shell around the solute molecule. When such motion dominates, the molecule is not well solvated and its transition energy is located on the red side of the absorption spectrum, in the case of IR140. On the other hand, inertial motion dominates in situations where the solvent shell is dense, i.e., when the molecule is well solvated. Thus, molecules such as IR140 absorb at shorter wavelength. For molecules with an absorption spectrum shifting to lower frequency with increasing solvent polarity, the opposite behavior is expected. This interpretation is supported by the solvent dependence of the solvation dynamics. Inertial motion is larger in solvents composed of small molecules, where the solute molecule is surrounded by a large number of polar heads, than in solvents composed of long molecules such as DeCN, where substantial reorientation of the polar head cannot occur without diffusive motion.

Such measurements might prove to be very fruitful for understanding more complex systems, such as chromophores embedded in a protein.

Acknowledgment. This work was supported by the Fonds national suisse de la recherche scientifique through Project 2000-055388.98. Financial support form the Fonds de la recherche and the Conseil de l'Université de Fribourg is also acknowledged.

References and Notes

(1) Porter, G.; Suppan, P. *Pure Appl. Chem.* **1964**, *9*, 499.
(2) Bagchi, B.; Oxtoby, D. W.; Fleming, G. R. *Chem. Phys.* **1984**, *86*, 257.
(3) Simon, J. D. *Acc. Chem. Res.* **1988**, *21*, 128.
(4) Barbara, P. F.; Jarzeba, W. *Adv. Photochem.* **1990**, *15*.
(5) Kivelson, D.; Friedman, H. *J. Phys. Chem.* **1989**, *93*, 7026.
(6) Maroncelli, M.; Fleming, G. R. *J. Chem. Phys.* **1988**, *89*, 5044.

(7) Rosenthal, S. J.; Xie, X.; Du, M.; Fleming, G. R. *J. Chem. Phys.* **1991**, *95*, 4715.
(8) Jimenez, R.; Fleming, G. R.; Kumar, P. V.; Maroncelli, M. *Nature* **1994**, *369*, 471.
(9) Goldberg, S. Y.; Bart, E.; Meltsin, A.; Fainberg, B. D.; Huppert, D. *Chem. Phys.* **1994**, *183*, 217.
(10) Fleming, G. R.; Cho, M. *Annu. Rev. Phys. Chem.* **1996**, *47*, 109.
(11) Berg, M.; Bout, D. A. V. *Acc. Chem. Res.* **1997**, *30*, 65.
(12) Tokmakoff, A.; Lang, M. J.; Larsen, D. S.; Fleming, G. R. *Chem. Phys. Lett.* **1997**, *272*, 48.
(13) de Boeij, W. P.; Pshenichnikov, M. S.; Wiersma, D. A. *Annu. Rev. Phys. Chem.* **1998**, *49*, 99.
(14) Lang, M. J.; Jordanides, X. J.; Song, X.; Fleming, G. R. *J. Chem. Phys.* **1999**, *110*, 5884.
(15) Vauthey, E.; Voss, J.; Caro, C. D.; Renn, A.; Wild, U. P. *J. Lumin.* **1993**, *56*, 61.
(16) Zollfrank, J.; Friedrich, J. *J. Phys. Chem.* **1992**, *86*, 7887.
(17) Vauthey, E.; Holliday, K.; Wei, C.; Renn, A.; Wild, U. P. *Chem. Phys.* **1993**, *171*, 253.
(18) Fleming, G. R. *Chemical Applications of Ultrafast Spectroscopy*; Oxford University Press: New York, 1986.
(19) Simon, J. D. *Pure Appl. Chem.* **1990**, *62*, 2243.
(20) Nishiyama, K.; Asano, Y.; Hashimoto, N.; Okada, T. *J. Mol. Liquids* **1995**, *65/66*, 41.
(21) Horng, M. L.; Gardecki, J. A.; Papazyan, A.; Maroncelli, M. *J. Phys. Chem.* **1995**, *99*, 17311.
(22) Joo, T.; Jia, Y.; Yu, J.-Y.; Lang, M. J.; Fleming, G. R. *J. Chem. Phys.* **1996**, *104*, 6089.
(23) Passino, S. A.; Nagasawa, Y.; Fleming, G. R. *J. Phys. Chem.* **1997**, *101*, 725.
(24) Gumy, J.-C.; Vauthey, E. *J. Phys. Chem.* **1996**, *100*, 8628.
(25) Perrin, D. D.; Armarego, W. L. F.; Perrin, D. R. *Purification of Laboratory Chemicals*; Pergamon Press: Oxford, 1980.
(26) Deeg, F. W.; Fayer, M. D. *J. Chem. Phys.* **1989**, *91*, 2269.
(27) Myers, A. B.; Hochstrasser, R. M. *IEEE J. Quantum Electron.* **1986**, *QE-22*, 1482.
(28) von Jena, A.; Lessing, H. E. *Appl. Phys.* **1979**, *19*, 131.
(29) Eichler, H. J.; Langhans, D.; Massmann, F. *Opt. Comm.* **1984**, *50*, 117.
(30) Etchepare, J.; Grillon, G.; Chambaret, J. P.; Hamoniaux, G.; Orzag, A. *Opt. Commun.* **1987**, *63*, 329.
(31) Cong, P.; Deuel, H. P.; Simon, J. D. *Chem. Phys. Lett.* **1993**, *212*, 367.
(32) Nelson, K. A.; Casalegno, R.; Miller, R. J. D.; Fayer, M. D. *J. Chem. Phys.* **1982**, *77*, 1144.
(33) Vauthey, E.; Henseler, A. *J. Phys. Chem.* **1995**, *99*, 8652.
(34) Högemann, C.; Vauthey, E. *Isr. J. Chem.* **1998**, *38*, 181.
(35) Lee, S. H.; Lee, J. H.; Joo, T. *J. Chem. Phys.* **1999**, *110*, 10969.
(36) Maroncelli, M.; Kumar, V. P.; Papazyan, A. *J. Phys. Chem.* **1993**, *97*, 13.
(37) Zolotov, B.; Gan, A.; Fainberg, B. D.; Huppert, D. *Chem. Phys. Lett.* **1997**, *265*, 418.